# Predicting the Optical Performance of the Space Interferometry Mission Using a Modeling, Testing, and Validation Methodology

**Ipek Basdogan**
Department of Mechanical Engineering,
Koc University,
Sariyer, Istanbul, 80910

**Laila Mireille Elias**
Space Systems Laboratory,
Massachusetts Institute of Technology,
Cambridge, MA 02139

**Frank Dekens**

**Lisa Sievers**

Jet Propulsion Laboratory,
California Institute of Technology,
Pasadena, CA 91109

*This paper presents the modeling, testing, and validation methodologies developed to predict the optical performance of the Space Interferometry Mission (SIM) at the Jet Propulsion Laboratory (JPL). The modeling methodology combines structural, optical, and control system design within a common state space framework and incorporates reaction wheel assembly (RWA) disturbances to evaluate the end-to-end performance of the system requirements. The validation methodology uses the Micro-Precision Interferometer (MPI) testbed, which is a ground-based, representative hardware model of SIM. In this study, the integrated model of the MPI testbed was used to calculate the transfer functions from RWA input to optical performance output. The model-predicted transfer functions were compared with the MPI testbed measurements, and the accuracy of the integrated model was quantified using a metric that was based on output power of the transfer functions. The RWA disturbances were then propagated through the modeled and measured transfer functions to predict the optical performance of the MPI testbed. This method is called the "decoupled disturbance analysis" and relies on the "blocked" RWA disturbances, measured with the RWA hardmounted to a rigid surface. These predictions were compared with the actual (measured) optical performance of MPI, measured with the RWA mounted to MPI, to evaluate the accuracy of the decoupled disturbance analysis method. The results show that this method is not an accurate representation of the coupled boundary conditions that occurs when the RWA is mounted to the flexible MPI structure. In order to correct for the blocked RWA disturbance boundary conditions, the "coupled disturbance analysis" method was developed. This method uses "force filters" that depend on estimates of the interface accelerances of the RWA and the MPI structure to effectively transform the blocked RWA disturbance measurements into their corresponding "coupled" disturbances (the disturbances that would occur at the coupled RWA-MPI interface). Compared to the decoupled method, the coupled method more accurately predicts the system's performance. Additionally, the RWA cross-spectral density terms were found to be influential in matching the performance predictions to the measured optical performance of MPI.* [DOI: 10.1115/1.2202152]

## 1 Introduction

NASA's Space Interferometry Mission (SIM) (see Fig. 1) will be the first space-borne interferometer; it is scheduled for launch in 2009. It will determine the positions and distances of stars several hundred times more accurately than any previous program. Interferometry is a technique in which the light from two collecting apertures is combined in order to achieve the equivalent resolution of a single telescope with a diameter equal to the separation distance of the two collecting apertures. When the light is combined properly, interference fringes can be measured by the instrument and the resulting data is used to measure the angular separation of multiple stellar objects. In order to ensure mission success, the optical path length difference (OPD) between the two telescopes or equivalently the stellar fringe position is required to be stabilized down to 10-nm root mean square (rms) in the presence of the on-board disturbances [1].

The primary disturbance source anticipated for SIM spacecraft is the reaction wheel assembly (RWA). Reaction wheels are momentum exchange devices, which are often used for spacecraft attitude control and for performing large angle slewing maneuvers. The RWA disturbances can be classified by their frequency content, magnitude level, location, and direction at which they enter the structure. It is important that accurate models of the SIM instrument and the RWA disturbances are available to predict the mission performance at the early design stages so that costly redesigns at later stages of the project are avoided.

Integrated modeling methodology development and validation has been one of the key activities of the SIM project to reduce the mission risks and to address these technological challenges. The integrated modeling methodology combines structural, optical, and control system design within a common software environment which enables an end-to-end performance evaluation of the system requirements. Coincident with the modeling development, the Micro-Precision Interferometer (MPI) testbed was built to assess vibration attenuation technologies on a dynamically and dimensionally representative hardware model of the SIM (see Fig. 2) [2,3]. An integrated model of MPI was developed in parallel with the testbed. This modeling and hardware synergy resulted in a unique opportunity to validate the modeling methodology by comparing model predictions with the testbed measurements. For a class of missions like SIM where end-to-end system level test is

Contributed by the Technical Committee on Vibration and Sound of ASME for publication in the JOURNAL OF VIBRATION AND ACOUSTICS. Manuscript received July 7, 2004; final manuscript received March 17, 2006. Assoc. Editor: John A. Main.

  

**Fig. 1 Space Interferometry Mission**

unavailable or unfeasible, the combination of modeling and technology testbeds is essential to reduce the performance risk.

This paper presents the validation of the OPD performance prediction method and studies the effect of the RWA disturbances on the OPD jitter. The OPD transfer functions (TF) were calculated using the integrated model of the MPI testbed and validated using the MPI measured transfer functions. After the transfer functions were validated, the performance of the instrument was measured when the MPI structure was subjected to the anticipated RWA disturbances. The RWA disturbances were measured in a "blocked" or "infinite-impedance" configuration, in which the RWA was hardmounted to a rigid surface and its interface was constrained to have zero motion. The RWA was spun, and load transducers were used to measure the resulting disturbance loads at the interface. The blocked RWA disturbances were then propagated through the measured and modeled transfer functions to predict the resulting OPD performance as a function of wheel speed. This prediction method is called the "*decoupled disturbance analysis method*," since the blocked RWA disturbances differ from those that would occur if the RWA were actually mounted to MPI. For the reaction wheel disturbance modeling there are a few existing studies in the literature. The most commonly used RWA disturbance model was created to predict the effects of the RWA induced vibrations on the Hubble Space Telescope [4]. Melody [5] developed discrete-frequency and broadband reaction wheel disturbance models to predict the performance of the SIM spacecraft with the decoupled disturbance analysis method. Masterson et al. [6] developed an empirical model of reaction wheel disturbances from steady state reaction wheel test data. This model was also used to predict the performance of the SIM spacecraft under the effect of the RWA disturbances [7].

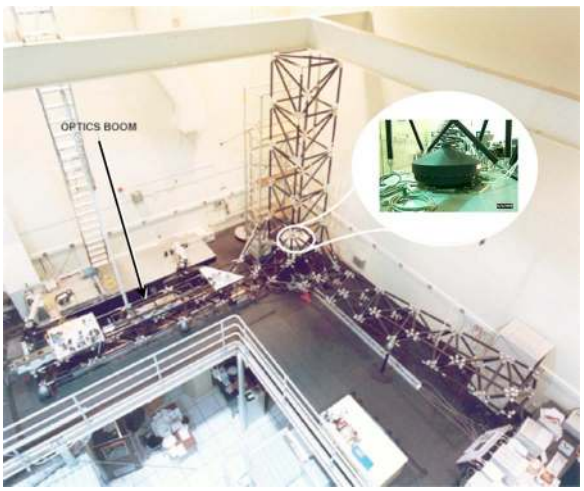


**Fig. 2 The MPI testbed with RWA in inset**

While the decoupled method provides consistent and repeatable conditions, they are not an accurate representation of the coupled boundary conditions that occur when the RWA is mounted to a flexible structure. Hence, this paper also presents techniques used to correct for the boundary conditions imposed on the RWA during blocked disturbance testing. "Force filters" were used to transform the blocked RWA disturbances into the corresponding coupled disturbances that would occur if the RWA were mounted to MPI. This method is called the "*coupled disturbance analysis method*" and the details will be described in Sec. 5.3. The coupled disturbances were then propagated, in place of blocked disturbances, through the MPI TF to predict the coupled performance. Both the decoupled and coupled analysis methods were validated by experimental data from the MPI testbed.

The actual OPD performance of the instrument can be measured directly while the wheel is spinning on MPI. It is called "true OPD" and is used as the basis for the validation studies conducted in this paper. This measurement is not feasible on the SIM spacecraft since the flight hardware will not be ready until the end of the implementation phase of the project. But instead, one can build an integrated model of the SIM spacecraft using the modeling methodology presented in this paper and apply the same disturbance analysis method to predict the OPD performance of the SIM instrument under the same type of RWA disturbances [7]. The validation techniques presented in this paper give us confidence in our modeling methodology which means that we can trust the predictions of the integrated models if the design changes over the course of the next 4 years.

## 2 The Micro-Precision Interferometer Testbed

The MPI testbed is used to validate the modeling methodologies presented in this paper. Active optics, located on the optics boom of the testbed are used to measure MPI's performance in the presence of vibrational disturbances induced at the base of the three booms by an on board RWA (see Fig. 2). In this study, the performance metric of interest is the OPD between the two paths of the optical interferometer, expressed in nanometers and measured at the fringe detector.

The RWA, shown hardmounted directly to the MPI base plate in Fig. 2 is similar to the one used for attitude control on the Magellan spacecraft. While the RWA is used to induce coupled, tonal disturbances characteristic of those expected on SIM, voice coil shakers are alternatively used to induce "pure," decoupled, white-noise forces and moments. These decoupled disturbances are useful for measuring the transfer functions from the six loads (three forces and three moments) at the RWA mounting location to the OPD.

## 3 End-To-End OPD Prediction Validation Procedure

The first step of the validation effort is the parallel process of building the testbed and the simulation model (see Fig. 3). This process has been a continuous effort during the development of the MPI testbed from a simple structure to a full-scale interferometer. Step 2 involves measuring and predicting the disturbance-input to OPD-output transfer functions (with disturbances entering at the RWA location) using the testbed and the integrated model, respectively. Step 3 represents the comparison of the model-predicted and testbed-measured transfer functions using a metric based on output power of the transfer functions. In step 4, the RWA is mounted to a rigid surface and spun, and the blocked

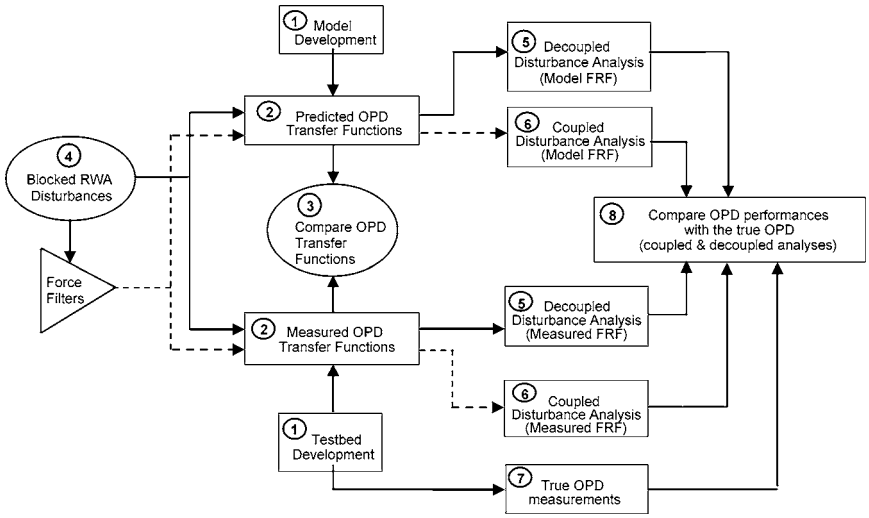


**Fig. 3 The OPD validation procedure**

RWA disturbances are measured. The blocked RWA disturbances are then propagated through the measured and modeled OPD transfer functions to predict the OPD performance. This is called the "decoupled disturbance analysis" and represented by step 5. As shown in the following sections, the blocked RWA testing condition used in the decoupled disturbance analysis does not accurately represent the coupled boundary conditions when the RWA is mounted to the flexible MPI structure. In order to correct the blocked boundary condition, force filters are used to impose coupled boundary conditions on the blocked RWA disturbances. As will be discussed in Sec. 5.3, force filters are calculated by modeling the accelerance of the RWA using a rigid-body model and the accelerance of MPI using a finite element model (FEM). This method is called the "coupled disturbance analysis" and is represented by step 6. The coupled disturbance analysis was further improved by including gyroscopic effects of the spinning flywheel in the rigid-RWA accelerance model, as well as previously neglected RWA disturbance cross-spectral-density terms. The actual OPD performance (true OPD, step 7) was measured while the wheel was spinning on MPI. The true OPD performance measurement was then compared to all the OPD predictions to evaluate the best approach for the RWA disturbance analysis methodology (step 8).

The following section presents the details of the MPI integrated model and summarizes the validation of the model using the testbed TF measurements.

## 4 MPI Integrated Model and Validation

The MPI integrated model consists of a structural finite element model and a linear optical model integrated together. The structural model is generated with Integrated Modeling of Optical Systems (IMOS) [8], whereas both IMOS and Modeling and Analysis for Controlled Optical Systems (MACOS) [9] are used to create the optical model. The integration and disturbance analysis are performed in MATLAB with the aid of IMOS functions.

**4.1 Structural Model.** The structural model is specified in IMOS as a finite element geometry, shown in Fig. 4. This geometry consists of plate, beam, truss, and rigid body elements, modeling the base truss structure and the components. The base truss structure is made up of three booms: a horizontal optics boom (along the *x-axis*), a vertical tower (along the *z-axis*), and a canted metrology boom (nearly along the *y-axis*). The components consist of inboard and outboard optics plates, a disturbance mount plate where the RWA may be attached (see Fig. 2 inset), two siderostat mounts, an optics cart containing an active delay line, the optics cart support structure, a passive delay line, and an external metrology beam launcher plate. The FEM uses 3094 degrees of freedom, of which 2158 are independent, and the rest are constrained using rigid body multipoint constraints.

The governing equation for the multiple degree of freedom system generated by the finite element analysis (FEA) is

$$\mathbf{M}\ddot{\mathbf{d}} + \mathbf{C}\dot{\mathbf{d}} + \mathbf{K}\mathbf{d} = \mathbf{F}\mathbf{u} \tag{1}$$

where **M**, **C**, and **K** are the system's mass, damping, and stiffness matrices, respectively. The vector **d** is the nodal displacements, **u** is the control input, and **F** is the influence matrix for **u**. Then the system in Eq. (1) is transformed to the modal coordinates as

$$\Phi^{\mathrm{T}}\mathbf{M}\Phi\ddot{\eta} + \Phi^{\mathrm{T}}\mathbf{C}\Phi\dot{\eta} + \Phi^{\mathrm{T}}\mathbf{K}\Phi\eta = \Phi^{\mathrm{T}}\mathbf{F}\mathbf{u} \tag{2}$$

where $\Phi$ is the modal transformation (or eigenvector) matrix and $\eta$ is the vector of modal coordinates [10]. Equivalently, Eq. (2) can be rewritten as

$$\mathbf{M}_{\mathbf{P}}\ddot{\eta} + \mathbf{C}_{\mathbf{P}}\dot{\eta} + \mathbf{K}_{\mathbf{P}}\eta = \mathbf{F}_{\mathbf{P}}\mathbf{u} \tag{3}$$

where $\mathbf{M}_{\mathrm{P}}$, $\mathbf{C}_{\mathrm{P}}$, $\mathbf{K}_{\mathrm{P}}$ are diagonal modal mass, damping and stiffness matrices, respectively. The modal damping factor is assumed to be 0.3% for the global flexible-body modes and 3% for the

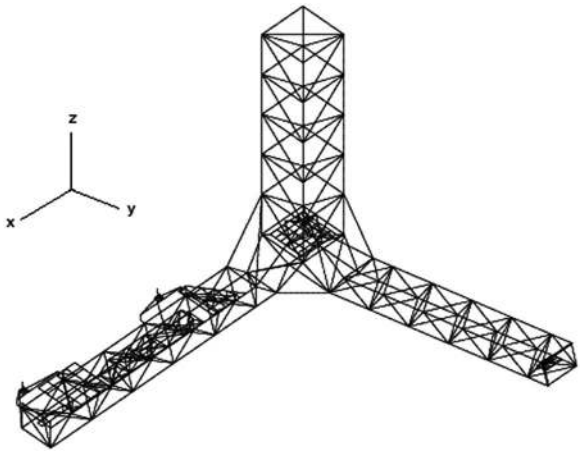


**Fig. 4 MPI finite element geometry**

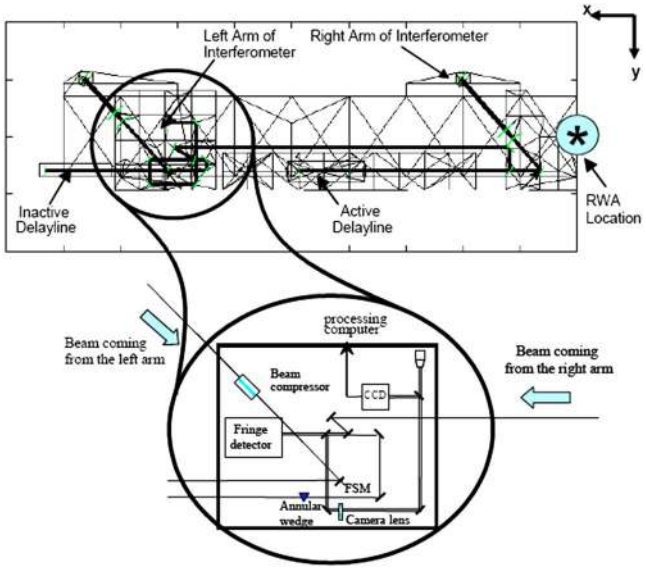


**Fig. 5 MPI optical raytrace on the finite element geometry of the optics boom**

dynamics associated with the delay line structure. These damping values are consistent with the estimates obtained from modal tests [11].

**4.2 Optical Model.** The optical model begins with a specification of the optical prescription. This prescription includes the shapes, positions, and orientations of the optical elements. A ray trace of the optical prescription is shown in Fig. 5. Note that Fig. 5 indicates the location of the optical sensor (fringe detector for the pathlength control system) and the location of the disturbance source (RWA). This optical prescription, together with the structural model, is generated in IMOS based on the layout of the actual optical elements on MPI. Optical model generation uses the structural finite element geometry where the optical elements are attached to the FEM nodes. From the FEA results, we can determine the new (perturbed) locations of the optical elements. This information is exchanged with the MACOS software to calculate the analytic differential ray trace [7]. The result is a model of the form:

$$\mathbf{y} = \mathbf{C}_{\text{opt}}\mathbf{d}_{\text{opt}} \tag{4}$$

where $\mathbf{d}_{\text{opt}}$ is a vector of optical element perturbations (i.e., a subset of $\mathbf{d}$ in Eq. (1)), $\mathbf{y}$ is a vector of optical output, and $\mathbf{C}_{\text{opt}}$ is the optical sensitivity matrix giving the change in ray state due to perturbations of the optical elements. Elements of the optical output vector can be pathlength difference, wave front tip/tilt, or beam sheer, depending on the analysis performed [12].

**4.3 Structural-Optical Model Integration.** First, the structural model is truncated to remove modes above the bandwidth of expected disturbances (i.e., above 1000 Hz). Then, the structural and optical models are integrated to form a structural-optical model in first-order, state-space form, such that

$$\begin{aligned} \dot{\mathbf{x}} &= \mathbf{A}\mathbf{x} + \mathbf{B}\mathbf{u} \\ \mathbf{y} &= \mathbf{C}\mathbf{x} \end{aligned} \tag{5}$$

where

$$\mathbf{A} = \begin{bmatrix} \mathbf{0} & \mathbf{I} \\ -\mathbf{M}_{\mathbf{P}}^{-1}\mathbf{K}_{\mathbf{P}} & -\mathbf{M}_{\mathbf{P}}^{-1}\mathbf{C}_{\mathbf{P}} \end{bmatrix}$$

$$\mathbf{B} = \begin{bmatrix} \mathbf{0} \\ \mathbf{M}_{\mathbf{P}}^{-1}\mathbf{F}_{\mathbf{P}} \end{bmatrix} \quad \text{and} \quad [\mathbf{C}] = [\mathbf{C}_{\text{opt}}\mathbf{\Phi}\ \mathbf{0}].$$

The state space form in Laplace domain allows the calculation of the transfer functions $\mathbf{G}(s)$, that relate the output OPD, $\mathbf{Y}(s)$, to the given RWA disturbance inputs, $\mathbf{U}(s)$, such that [13]

$$\mathbf{G(s)} = \frac{\mathbf{Y(s)}}{\mathbf{U(s)}} \tag{6}$$

Inputs are defined at disturbance locations and actuated degrees of freedom for the articulated optical surfaces, whereas outputs are measured at the fringe detectors and the wave front tilt cameras. These transfer functions depict how the disturbance propagates from the disturbance source to the optical sensor. The transfer functions for all disturbance directions (three forces and three moments at each disturbance input node) are obtained using the standard MATLAB functions after the state space model is built.

**4.4 MPI Disturbance Transfer Function Measurement and Validation.** In this study, disturbance-input to OPD-output transfer functions are measured to validate the modeled transfer functions, which should characterize the propagation of the disturbances to OPD. Figure 5 shows the disturbance input location and the OPD output location (fringe detector) on the MPI testbed.

A pair of 10 N shakers mounted on a custom six-axis force measuring device (dynamometer) is used as the disturbance source. A HP data analyzer is used to drive the shakers, record the dynamometer and fringe measurements, and calculate the transfer function. The disturbance transfer functions were measured for three force and three moment disturbance directions: $F_x, F_y, F_z, M_x, M_y, M_z$.

The fringes only occur when the optical pathlength from the star through the left interferometer arm (all the way to the combination point in the beam combiner) is equal to the optical path traversed through the right interferometer arm. To make this equalization possible, an active optical delay line is added to one arm of the interferometer in order to extend or shorten the optical path of that arm as needed. Once the delay line is set to a position where the paths are exactly equal, the angle to the star can be determined by measuring critical distances in the interferometer. These measurements are accomplished with the metrology subsystem. A fringe detector is then used to measure the difference between the two interferometer arms. This can then be used as the output signal to a signal analyzer.

The measured and predicted transfer functions are compared utilizing a metric that was developed for previous validation studies [14]. This metric, $\sigma_g$, is the square root of the output variance resulting from a band-limited white noise input

$$\sigma_g^2 = \frac{A_d}{\pi}\int_{f_{min}}^{f_{max}} |G(\omega)|^2 d\omega \tag{7}$$

where $A_d$ is the amplitude of the band-limited white noise disturbance power spectral density, and $\mathbf{G}(\omega)$ is the transfer function from Eq. (16). The frequency range of interest is defined by $f_{\text{min}}$ and $f_{\text{max}}$.

Using this metric, the accuracy of the model can be quantified by comparing $\sigma_g$ of the predicted and measured transfer functions. Note that, $\sigma_g$ has no significance by itself. It is the comparison of metrics for corresponding measured and predicted transfer functions. The measured transfer functions, along with the corresponding predicted transfer functions, are shown in Fig. 6.

The results of these comparisons are shown in Table 1. The table entries represent the ratio of $\sigma_g$ between the measured and predicted transfer functions for a number of bandwidths of interest between 4 and 1000 Hz. Below 4 Hz the force capability of the shakers are limited and the testbed suspension modes pollute the

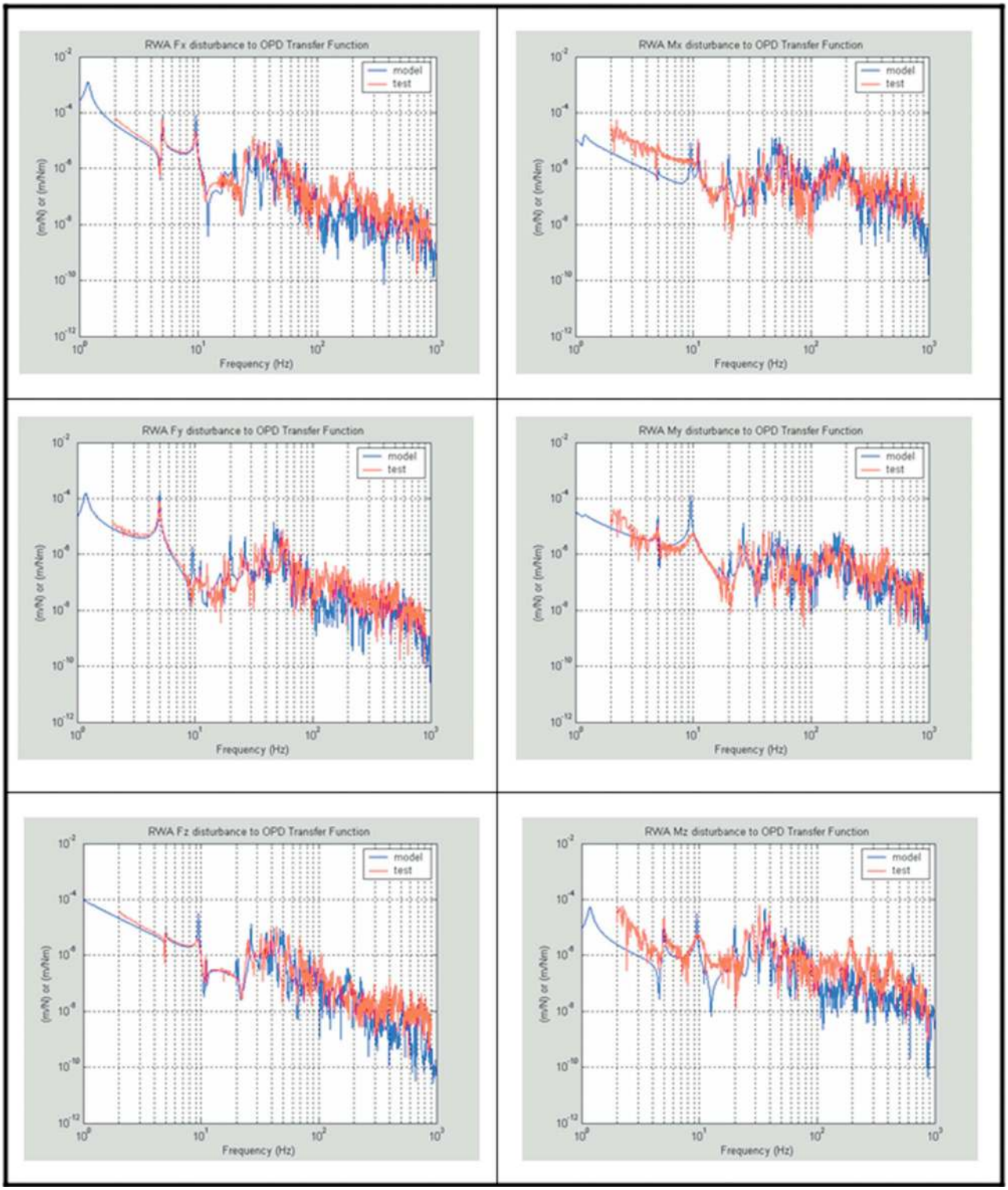


**Fig. 6 Measured and FEM-modeled MPI transfer functions: RWA disturbances to OPD**

measurement. Above 1000 Hz, MPI measurements are limited by background noise. This bandwidth is broken down into decades for comparison purposes.

As it can be seen from the last column of Table 1, the integrated model predicts the OPD within a factor of 2 over the entire 4–1000 Hz range (except for the *y*-axis moment disturbance input). Matching the predicted and measured TFs peak-to-peak is a very tedious process for structures like MPI, since it includes many flexible and damped components that are difficult to model. In Fig. 6, the measured TF peaks appear much more "damped" than the modeled TF peaks, and some of the peaks are not located at the right frequencies. Although the accuracy of the model is considered to be very good except the disturbance about the *y*-axis, the mismatch between measured and modeled TFs will obviously have an impact on the resulting OPD predictions in the following sections. The discrepancies between the predicted and the measured transfer functions are mainly due to the errors made in the modeling.

**Table 1 Metric comparison between the predicted and measured transfer functions for the MPI testbed**

| Disturbance Input | $\sigma_g$ predicted/$\sigma_g$ measured 4–10 Hz | 10–100 Hz | 100–1000 Hz | 4–1000 Hz |
|---|---|---|---|---|
| $F_x$ | 1.46 | 0.84 | 0.19 | **1.25** |
| $F_y$ | 1.30 | 1.59 | 0.31 | **1.33** |
| $F_z$ | 1.56 | 1.10 | 0.49 | **1.24** |
| $M_x$ | 0.40 | 1.88 | 0.97 | **1.29** |
| $M_y$ | 5.81 | 1.30 | 1.02 | **2.48** |
| $M_z$ | 1.30 | 0.79 | 0.17 | **0.78** |

## 5 RWA Disturbance Analysis Method and Validation

**5.1 Decoupled Disturbance Analysis Method.** The "decoupled" disturbance analysis method is based on a simple frequency-domain input-output principle. The MPI OPD is predicted for each wheel speed, $\Omega$, as [15]

$$Z(\omega,\Omega) = G_{ZF}(\omega)F(\omega,\Omega) \tag{8}$$

where $\omega$ represents frequency (in units of radians per second), $Z$ is the "predicted performance" vector (in this case, the scalar OPD), $F$ is disturbance load vector (in this case, the $6\times1$ vector of measured RWA disturbance forces and moments). $G_{ZF}$ is the TF of the structure as defined in Eq. (6) (in this case, the $1\times6$ TF vector relating disturbance forces and moments at the RWA mounting location on MPI to the OPD). In this paper, $G_{ZF}$ is obtained both from the MPI integrated model and from the MPI testbed (yielding the measured and modeled TFs, respectively). Taking the expectation of the "square" of Eq. (8) allows us to write the disturbance analysis equation in terms of spectral density matrices

$$\Phi_{ZZ}(\omega,\Omega) = G_{ZF}(\omega)\Phi_{FF}(\omega,\Omega)G_{ZF}^{*\mathrm{T}}(\omega) \tag{9}$$

where $\Phi_{ZZ}$ is the output performance spectral density matrix (in this case, the scalar OPD power spectral density), $\Phi_{FF}$ is the RWA disturbance spectral density matrix (in this case, the $6\times6$ matrix with disturbance force and moment power spectra on the diagonal and cross-spectra off the diagonal), and $[.]^{*\mathrm{T}}$ denotes a complex conjugate transpose operation.

It is assumed that the diagonal terms of $\Phi_{FF}$, or power spectral densities (PSDs), dominate the off-diagonal terms, or cross-spectral densities (CSDs)

$$\Phi_{F_iF_i} \gg |\Phi_{F_iF_j}|, \quad i \neq j \tag{10}$$

When this holds true, $\Phi_{FF}$ is approximated as a diagonal matrix, and Eq. (9) reduces from a fully populated matrix equation to a simple *summation of diagonal terms*

$$\Phi_{ZZ}(\omega,\Omega) \approx \sum_{j=1}^{6} \Phi_{F_iF_i}(\omega,\Omega)|G_{Z_iF_i}(\omega)|^2 \tag{11}$$

From Eq. (11), we may calculate the rms, $\sigma_z$, of the performance, $Z$, for each wheel speed, $\Omega$

$$\sigma_z(\Omega) = \sqrt{2\int_0^{\omega_{\max}} \Phi_{ZZ}(\omega,\Omega)d\omega} \tag{12}$$

For each wheel speed, $\Omega$, the OPD spectrum, $\Phi_{ZZ}$ is approximated using Eq. (11), and the its rms is calculated using 12. To validate these predictions, the true OPD of the coupled MPI-RWA system is measured for each wheel speed with the RWA mounted on MPI. Figure 7 shows the measured OPD rms versus the predicted OPD rms (using both measured and modeled transfer functions), both as functions of wheel speed.

**5.2 Motivation for a Coupled Disturbance Analysis Method.** The work in the remainder of this paper is motivated by the fact that the predicted MPI OPD in Fig. 7 does not agree with

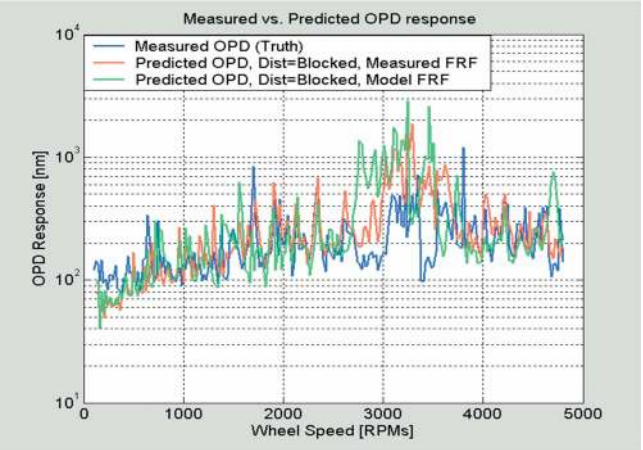


**Fig. 7 Measured versus predicted OPD response using blocked RWA disturbances. (Note that the predicted OPD is calculated using both measured and modeled transfer functions.)**

the measured OPD. The discrepancy has been, up to now, attributed to the decoupled nature of the disturbance analysis method in Eq. (11). In propagating blocked RWA disturbances (described in Sec. 3) through a modeled or measured MPI transfer function, this method neglects the structural dynamic coupling between the MPI and the RWA.

RWA disturbances are typically measured in a blocked configuration, in which the RWA is hardmounted to a rigid surface. The RWA is spun while its interface is constrained to have zero motion, and load cells are used to measure the resulting disturbance loads at the rigid interface. This is known as an "infinite-impedance" boundary condition and is quite different from the actual RWA interface impedance when it is coupled to a spacecraft. This inaccurate set of boundary conditions effectively neglects the coupling of the MPI-RWA system, and it is thought to be a critical approximation in the decoupled disturbance analysis method. This study accounts for this mismatch in RWA disturbance-testing boundary conditions by applying a coupling theory to the performance predictions on MPI.

It is important to note that in the past, predictions have overbounded measurements by up to a factor of four, significantly more than shown in Fig. 7. Recent hardware modifications have "stiffened" the MPI-RWA interface, which in turn both decreased the amount of overprediction and confined it primarily to the range of wheel speeds between 2700 and 3700 revolutions per minute (rpm). This confirms that dynamic coupling may be a critical issue being neglected in the decoupled disturbance analysis method, since stiffening the interface effectively decreases the dynamic coupling between the two bodies, thus improving the decoupled prediction.

Another indication that coupling is a concern is the fact that the OPD predicted using coupled RWA disturbances (measured with the RWA mounted to MPI) in place of blocked disturbances (measured with the RWA mounted to a rigid steel block) yields much better results. Figure 8 shows that using the coupled disturbances dramatically improves the OPD prediction at 2700–3200 and 3400–3500 rpm, particularly when using the *measured* MPI transfer functions.

Since there are still some small regions in Fig. 8 where the predictions do not match the truth (such as 3200–3400 and 3500–3700 rpm), we must also consider other factors that could be contributing to errors in the OPD prediction. Aside from neglecting dynamic coupling between the MPI and RWA, the disturbance analysis method in Eq. (11) makes other mathematical and physical approximations. Recall that we are neglecting the RWA disturbance CSD terms in the transition from Eqs. (9)–(11). Additionally, Eq. (11) fails to account for the gyroscopic stiffening effects

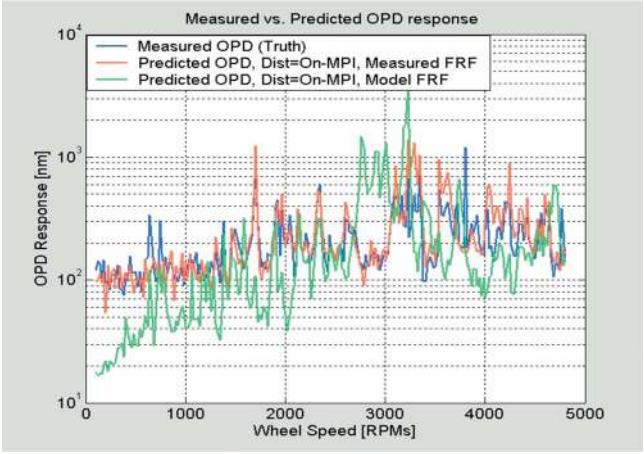


**Fig. 8 Measured versus predicted OPD response *using on-MPI RWA disturbances***

of the spinning RWA. A secondary goal of this work is to assess the effect of these approximations. The gyroscopic and off-diagonal approximations will be addressed in Secs. 5.4 and 5.5, respectively.

**5.3 Force Filter Coupling Method.** We will develop a force filter approach to correct the mismatch of boundary conditions that occurs when measuring RWA disturbances in a blocked configuration. The force filter is a method of transforming (or "filtering") dynamic loads measured on a *fixed* structure (such as a hardmounted RWA) to the equivalent loads that would exist if the structure were interfaced instead with another flexible body. The force filter is therefore a function of the dynamics of both bodies.

The force filter for the $i$th axis may be expressed as [15,16]

$$\tilde{G}_{f,ii}(\omega) \equiv \frac{F_{c,i}(\omega)}{F_{b,i}(\omega)} = \frac{1}{1+\dfrac{A_{\mathrm{MPI},ii}(\omega)}{A_{\mathrm{RWA},ii}(\omega)}}, \quad i=1,2,3 \tag{13}$$

where $i=1,2,3$ refers to the $x$, $y$, and $z$ axes, respectively, $\omega$ represents frequency in radians per second, $F_{c,i}$ is the Fourier transform of the coupled interface force along the $i$th axis, $F_{b,i}$ is the Fourier transform of the measured blocked force along the $i$th axis, $A_{\mathrm{MPI},ii}$ is the MPI driving-point accelerance along the $i$th axis, and $A_{\mathrm{RWA},ii}$ is the RWA driving-point accelerance along the $i$th axis.

Similarly, a "moment filter" may be expressed as

$$\tilde{G}_{f,ii}(\omega) \equiv \frac{M_{c,i}(\omega)}{M_{b,i}(\omega)} = \frac{1}{1+\dfrac{A_{\mathrm{MPI},ii}(\omega)}{A_{\mathrm{RWA},ii}(\omega)}}, \quad i=4,5,6 \tag{14}$$

where $i=4,5,6$ refers to rotations about the $x$, $y$, and $z$ axes, respectively. $M_{c,i}$ is the Fourier transform of the coupled interface moment along the $i$th axis, $M_{b,i}$ is the Fourier transform of the measured blocked moment along the $i$th axis, $A_{\mathrm{MPI},ii}$ is the MPI driving-point rotational accelerance about the $i$th axis, and $A_{\mathrm{RWA},ii}$ is the RWA driving-point rotational accelerance about the $i$th axis.

Table 2 provides a compilation of terms describing the generalized input-output relationships between a load imparted on a body and its corresponding position, velocity, and acceleration [17,18]. From this table it is clear that accelerance, $A$, is simply a derivative of mobility, $Y$ [18]

$$A(\omega) = \frac{\ddot{Q}(\omega)}{F(\omega)} = \frac{j\omega\dot{Q}(\omega)}{F(\omega)} = j\omega Y(\omega) \tag{15}$$

so that a ratio of the accelerances of the two bodies is equivalent to a ratio of their mobilities

**Table 2 Generalized input-output relationships between a load ($F$) on a body and the displacement ($Q$), velocity ($\dot{Q}$), and acceleration ($\ddot{Q}$) of that body**

| Response/Load Ratios | | Load/Response Ratios | |
|---|---|---|---|
| $\alpha(\omega)=\frac{Q(\omega)}{F(\omega)}$ | **Receptance** | $\frac{1}{\alpha(\omega)}=\frac{F(\omega)}{Q(\omega)}$ | Dynamic Stiffness |
| $Y(\omega)=\frac{\dot{Q}(\omega)}{F(\omega)}$ | Admittance<br>Mobility | $Z(\omega)=\frac{F(\omega)}{\dot{Q}(\omega)}$ | Mechanical Impedance |
| $A(\omega)=\frac{\ddot{Q}(\omega)}{F(\omega)}$ | **Accelerance** | $\frac{1}{A(\omega)}=\frac{F(\omega)}{\ddot{Q}(\omega)}$ | **Apparent Mass** |
| | Inertance | | Dynamic Mass |

$$\frac{A_{\mathrm{MPI},ii}}{A_{\mathrm{RWA},ii}} = \frac{j\omega Y_{\mathrm{MPI},ii}}{j\omega Y_{\mathrm{RWA},ii}} = \frac{Y_{\mathrm{MPI},ii}}{Y_{\mathrm{RWA},ii}} \tag{16}$$

Hence, the force and moment filters in Eqs. (13) and (14), respectively, which depend on the ratio of MPI and RWA accelerances, may be written equivalently as a function of MPI and RWA mobilities

$$\tilde{G}_{f,ii}(\omega) \equiv \frac{F_{c,i}(\omega)}{F_{c,i}(\omega)} = \frac{1}{1+\dfrac{Y_{\mathrm{MPI},ii}(\omega)}{Y_{\mathrm{RWA},ii}(\omega)}} = \frac{1}{1+\dfrac{A_{\mathrm{MPI},ii}(\omega)}{A_{\mathrm{RWA},ii}(\omega)}}, \quad i=1,2,3 \tag{17}$$

$$\tilde{G}_{f,ii}(\omega) \equiv \frac{M_{c,i}(\omega)}{M_{b,i}(\omega)} = \frac{1}{1+\dfrac{Y_{\mathrm{MPI},ii}(\omega)}{Y_{\mathrm{RWA},ii}(\omega)}} = \frac{1}{1+\dfrac{A_{\mathrm{MPI},ii}(\omega)}{A_{\mathrm{RWA},ii}(\omega)}}, \quad i=4,5,6 \tag{18}$$

If we now take the product of each blocked RWA disturbance force and moment with its corresponding force or moment filter (Eqs. (17) and (18)), we effectively filter the blocked disturbances to yield the coupled disturbances. We can thus transform the decoupled disturbance analysis equation, (11), into a coupled analysis equation

$$\Phi_{ZZ}(\omega,\Omega) \approx \sum_{j=1}^{6} \Phi_{F_iF_i}(\omega,\Omega)|\tilde{G}_{f,ii}(\omega)|^2|G_{ZF_i}(\omega)|^2 \tag{19}$$

where the first two terms represent the filtered, or coupled, RWA disturbance PSDs. Using the coupled equation, (19), in place of the decoupled equation, (11), effectively corrects the mismatch of boundary conditions imposed on $\Phi_{FF}$ by the blocked RWA disturbance testing.

In the case that force filters are available but moment filters are not (due to the difficulty in measuring rotational accelerances), Eq. (19) can be approximated by

$$\Phi_{ZZ}(\omega,\Omega) \approx \sum_{j=1}^{3} \Phi_{F_iF_i}(\omega,\Omega)|\tilde{G}_{f,ii}(\omega)|^2|G_{ZF_i}(\omega)|^2 + \sum_{j=4}^{6} \Phi_{F_iF_i}(\omega,\Omega) \times|G_{ZF_i}(\omega)|^2 \tag{20}$$

where moment filters have been set to unity, so that forces are filtered but moments are not.

Various methods have been identified to determine (measure or model) the MPI and RWA accelerances [15]. In this study, we use the FEM of MPI (see Sec. 4.1) and a rigid-body model of the RWA to estimate the desired translational and rotational accelerances of each body [15]. The resulting force and moment filters are used to generate a coupled disturbance analysis OPD prediction (see Fig. 9). Figure 9 demonstrates that the coupled prediction makes significant improvements to the decoupled prediction (Fig. 7) between 3050 and 3200 rpm, as well as between 3380 and 3520 rpm for the measured transfer functions. The coupled ap-

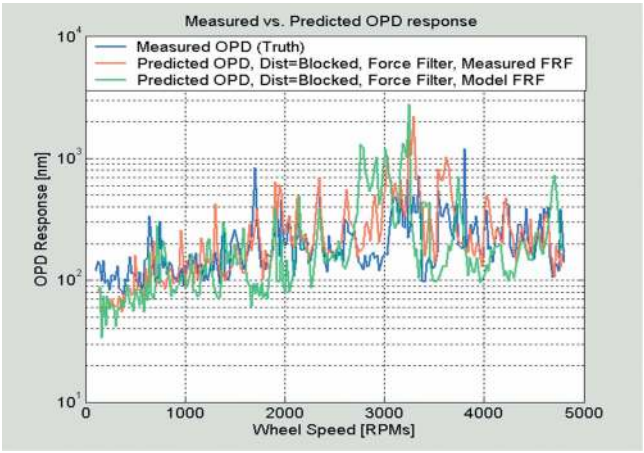


**Fig. 9 Measured versus predicted OPD response using blocked RWA disturbances *with force and moment filters***

proach does not improve the matching between the truth and the predicted OPD for the modeled transfer functions. This discrepancy can be explained by the differences between the modeled and the measured transfer functions (see Sec. 4.4 for details).

When Figs. 7–9 are analyzed carefully, they all show 100–1000 nanometer OPD performance which is significantly larger than the 10 nm requirement for the SIM instrument. Higher OPD predictions can be explained by the reaction wheel being directly mounted on the structure (hardmounted case). On the SIM spacecraft, there will be isolators between the reaction wheel and the structure to decrease the effect of the disturbances coming from the wheel locally. So when we add an isolator between the RWAs and the MPI structure, these numbers should decrease. Besides the specific reaction wheel that is used in this study is much noisier than the wheels that are going to be used on the SIM spacecraft.

**5.4 Gyroscopic Effects.** The MPI and RWA accelerances used to form the filters in Sec. 5.3 (using Eqs. (13) and (14) are independent of wheel speed. Clearly, the MPI accelerance is independent of wheel speed, yet this is not true for the RWA accelerance. In actuality, the RWA accelerance is influenced by gyroscopic effects, which depend directly on the wheel's spin rate. An attempt is now made to account for "gyroscopic stiffening" effects previously neglected in the rigid-body RWA accelerance model.

Consider a rigid, axially symmetric flywheel (a "disk") that spins at a rotational rate $\Omega$ about its axis of symmetry. The linearized rotational equations of motion of the flywheel about its radial axes are 15

$$\begin{bmatrix} I_{rr} & 0 \\ 0 & I_{rr} \end{bmatrix} \begin{Bmatrix} \ddot{\theta}_x \\ \ddot{\theta}_y \end{Bmatrix} + \begin{bmatrix} 0 & \Omega(I_{zz}-I_{rr}) \\ -\Omega(I_{zz}-I_{rr}) & 0 \end{bmatrix} \begin{Bmatrix} \dot{\theta}_x \\ \dot{\theta}_y \end{Bmatrix} = \begin{Bmatrix} m_x \\ m_y \end{Bmatrix} \tag{21}$$

where $I_{rr}$ is the mass moment of inertia about any radial axis, $I_{zz}$ is the mass moment of inertia about the spin axis, $\theta_x$ and $\theta_y$ are the angular rotations about the $x$ and $y$ axes, respectively, and $m_x$ and $m_y$ are external moments applied about the $x$- and $y$-axes, respectively. Notice the skew-symmetric damping matrix with two off-diagonal, wheel-speed-dependent terms: $\Omega I_{zz}$ and $-\Omega I_{zz}$. These are the gyroscopic terms of interest.

Taking the Fourier transform of Eq. (21), then using (15) to write velocities in terms of accelerations, collecting terms, and inverting, we solve to yield the flywheel's rotational accelerations in terms of the moments

$$\begin{Bmatrix} \ddot{\theta}_x \\ \ddot{\theta}_y \end{Bmatrix} = \begin{bmatrix} I_{rr} & \dfrac{\Omega(I_{zz}-I_{rr})}{j\omega} \\ \dfrac{-\Omega(I_{zz}-I_{rr})}{j\omega} & I_{rr} \end{bmatrix}^{-1} \begin{Bmatrix} M_x \\ M_y \end{Bmatrix} \tag{22}$$

so that the coupled rotational accelerances of the wheel about its $x$- and $y$-axes are

$$\begin{bmatrix} I_{rr} & \dfrac{\Omega(I_{zz}-I_{rr})}{j\omega} \\ \dfrac{-\Omega(I_{zz}-I_{rr})}{j\omega} & I_{rr} \end{bmatrix}^{-1} = \frac{1}{I_{rr}^2 - \left[\dfrac{\Omega}{\omega}(I_{zz}-I_{rr})\right]^2} \begin{bmatrix} I_{rr} & \dfrac{-\Omega(I_{zz}-I_{rr})}{j\omega} \\ \dfrac{\Omega(I_{zz}-I_{rr})}{j\omega} & I_{rr} \end{bmatrix} \tag{23}$$

We approximate the RWA accelerances in Eq. (23) by only the diagonal terms.[1] These terms are then used with Eq. (14) to form moment filters that include the gyroscopic effects of the RWA.

Figure 10 shows the coupled OPD prediction using the force and moment filters with RWA gyroscopic effects, as well as the measured OPD. Comparing this prediction to the decoupled OPD prediction from Sec. 5.1 (Fig. 7), the predictions due to the gyroscopic filters in Fig. 10 appear virtually indistinguishable from those due to the non gyroscopic filters in Fig. 9, indicating that, for this system, the inclusion of RWA gyroscopic effects in the moment filters does not yield a significant improvement to the performance prediction. We note that for a RWA with a very different ratio of inertias, or for a RWA that spins at much faster spin rates than those considered here, the gyroscopic dynamics may become influential. Hence although they may be neglected in the present results, we have developed an analysis method that includes these dynamics in case they are influential in other systems.

**5.5 Addition of CSD Disturbance Terms.** One final approximation in the decoupled disturbance analysis method is now investigated. Recall the simplification from the coupled matrix equations, (9), to the scalar equation, (11). The latter equation neglects the off-diagonal terms (CSDs) in the RWA disturbance spectral density matrix, $\Phi_{FF}$.

To investigate the effect of the disturbance CSDs (without accounting for coupling), a decoupled analysis including CSDs was performed using Eq. (9). The resulting OPD prediction is shown in Fig 11, along with the measured OPD. Comparing this prediction to the OPD prediction without CSDs from Sec. 5.1 (Fig. 7), we find that including the disturbance CSDs improves the decoupled OPD prediction in some regions (particularly near 2700–3000 and 3450–3550 rpm), yet degrades the prediction in other regions (such as near 2500–2600 and 3500–3600 rpm). Since this

[1]This approximation is necessary in order for the gyroscopic RWA accelerance model to fit into the existing force filter framework, as described by Eqs. (13) and (14). The effect of the neglected off-diagonal accelerance terms on the coupled OPD prediction will be investigated in the future.

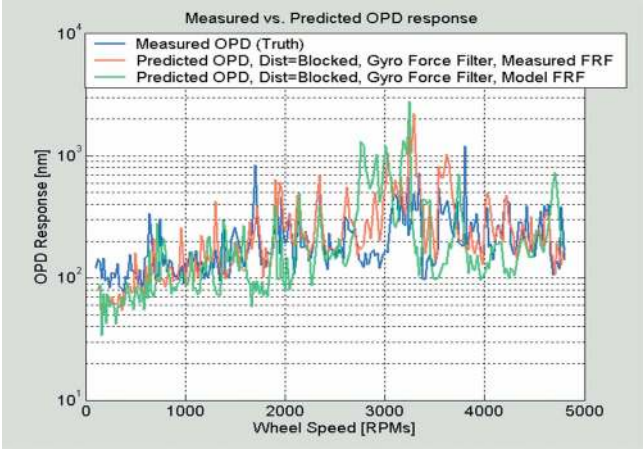


**Fig. 10 Measured versus predicted OPD response using blocked RWA disturbances *with gyroscopic-RWA force and moment filters***

is a decoupled prediction (without force filters), and the improvement is due simply to the addition of disturbance CSDs, it is recommended in future analyses (whether decoupled or coupled) to include RWA disturbance CSDs in the analysis equations.

## 6 Discussion and Conclusion

We presented a modeling, testing and validation methodology to predict the optical, performance of the Space Interferometry Mission. The integrated modeling strategy combines structural, optical, and control system modeling within the same software environment and allows the calculation of the transfer functions from various disturbance sources to optical performance outputs. The model predictions were validated utilizing the measured transfer functions obtained from the MPI testbed. The validation procedure is based on a calculation which quantifies the differences between the analytical and experimental transfer functions across a number of bandwidths. The integrated model predicts the OPD within a factor of 2 over the entire 4–1000 Hz range. The discrepancies between the model and measured transfer functions are caused by the inaccuracies in the modeling assumptions.

Experimental validation of this performance prediction method on the MPI testbed indicates that both the decoupled and the coupled analysis methods presented in this paper provide reasonable accuracy compared to measured performances. However, the coupled analysis method provides improved results, especially in certain wheel-speed ranges where MPI-RWA coupling is influential. The RWAs will likely spin primarily within a 20 rps (1200 rpm) window, and this window may be carefully selected to avoid certain ranges that cause detrimental performance of the interferometer. The coupled method does not improve the performance prediction for the modeled transfer functions. This behavior can be explained by the mismatch between the modeled and measured transfer functions.

Although a method was presented to include the gyroscopic nature of the spinning RWA in the RWA accelerance model, this additional model fidelity did not improve the performance predictions for the MPI-RWA system. However, for systems in which a RWAs gyroscopic dynamics are more influential, this method may prove useful.

Finally, the inclusion of RWA disturbance CSDs in Sec. 5.5 improves the OPD prediction significantly in certain regions, despite adversely affecting the prediction in other localized regions. Hence they are clearly not negligible and should be considered in future disturbance analyses.

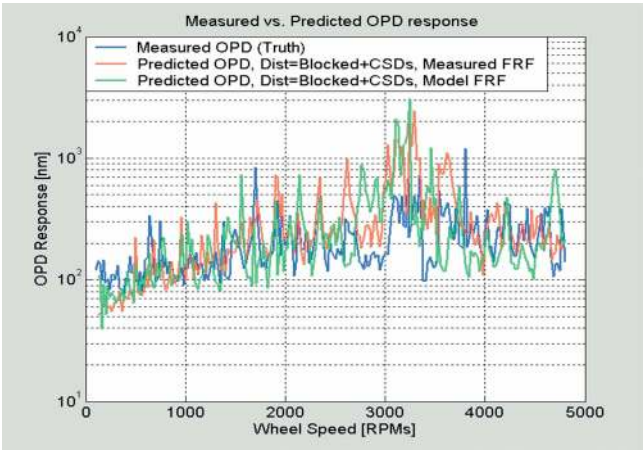


**Fig. 11 Measured versus predicted OPD response using blocked RWA disturbances *including* CSDs**

## Acknowledgment

Part of this work was carried out at Jet Propulsion Laboratory by the primary author under contract with the National Aeronautics and Space Administration.

## Nomenclature

CSD = cross-spectral density ($N^2$/Hz)
FEM = finite element model
MPI = micro-Precision Interferometer
OPD = optical pathlength difference
PSD = power spectral density ($N^2$/Hz)
rms = root mean square
rpm = revolutions per minute
rps = revolutions per second
RWA = reaction wheel assembly
SIM = Space Interferometry Mission
TF = transfer function

## References

[1] Shao, M., and Wolf, D. M., 1995, "Orbiting Stellar Interferometer," *Proceedings of SPIE Symposium on Spaceborne Interferometry*, Orlando, FL, April, Vol. 2447, pp. 228–239.
[2] Neat, G. W., Abramovici, A., Melody, J. W., Calvet, R. J., Nerheim, N. M., and O'Brien, J. F., 1997, "Control Technology Readiness for Spaceborne Optical Interferometer Missions," *Proceedings of Space Microdynamics and Accurate Control Symposium*, Toulouse, France, May.
[3] Basdogan, I., Dekens, F., and Neat, G. W., 1999, "A Model Validation Study of the Wave Front Tip/Tilt System Using the Micro-Precision Interferometer," *Proceedings of the IEEE Aerospace Conference*, Snowmass, CO, April.
[4] Hasha, M. D., 1986, "Reaction Wheel Mechanical Noise Variations," Space Telescope Program Engineering Memo SSS 218, June.
[5] Melody, J. W., 1995, "Discrete Frequency and Broadband Reaction Wheel Disturbance Models." JPL Interoffice Memo No. 3411-95-200csi, Internal Document, June.
[6] Masterson, R. A., 1999, "Development of Empirical and Analytical Reaction Wheel Disturbance Models," AIAA/ASME/ASCE/AHS/ASC Structures, Structural Dynamics and Materials Conference, St. Louis, MO.
[7] Basdogan, I., Grogan, R., Kissil, A., Sigrist, N., and Sievers, L., 2000, "Preliminary Optical Performance Analysis of the Space Interferometer Mission Using an Integrated Modeling Methodology," *Proceedings of the 6th Biennial Symposium on Active Control of Vibration and Noise, The 2000 International Mechanical Engineering Congress and Exposition*, Orlando, FL, Nov.
[8] Milman, M. H., Briggs, H. C., Ledeboer, W., Melody, J. W., Norton, R. L., and Needels, L., 1995, Integrated Modeling of Optical Systems User's Manual, Release 2.0, JPL D-13040, Internal Document, Nov.
[9] Redding, D., 1992, Controlled Optics Modeling Package User Manual, Release 1.0, JPL D-9816, internal document, June.
[10] Shabana, A. A., 1991, *Theory of Vibration*, Springer-Verlag, New York, Vol. 2.
[11] Levine-West, M. B., and Melody, J. W., 1995, "Model Updating of Evolutionary Structures," *Proceedings of 15th ASME Biennial Conference on Mechanical Vibration and Noise*, Boston, MA, Sept.

[12] Hecht, E., 1998, *Optics*, 3rd ed., Addison Wesley, Reading, MA.
[13] Kwon, Y. W., and Bang, H., 1997, *The Finite Element Method Using MATLAB*, CRC Press, Cleveland.
[14] Melody, J. W., and Neat, G. W., 1996 "Integrated Modeling Methodology Validation Using the Micro-Precision Interferometer Testbed," *Proceedings of 35th IEEE Conference on Decision and Control*, Kobe, Japan, Vol. 4, pp. 4222–4227, Dec.
[15] Elias, L., Dekens, F., Basdogan, I., Sievers, L., and Neville, T., 2002, "A Methodology for Modeling the Mechanical Interaction Between a Reaction Wheel and a Flexible Structure," *Proceedings of SPIE Astronomical Telescopes and Instrumentation Conference*, Waikoloa, HI.
[16] Ploen, S. R., 2001, "Analysis of MPI/RWA Dynamic Coupling via Mechanical Impedance Methods," Jet Propulsion Laboratory Engineering Memorandum 3455-01-001, January 4.
[17] Ewins, D. J., 2001, *Modal Testing: Theory, Practice, and Application*, 2nd ed., Research Studies Press.
[18] Elias, L. M., and Miller, D. W., 2002, "A Coupled Disturbance Analysis Method Using Dynamic Mass Measurement Techniques." *Proceedings of the 43rd Annual AIAA/ASME/ASCE/AHS/ASC Structures, Structural Dynamics, and Materials Conference*, Denver, CO, April 22–25, AIAA Paper No. 2002-1252.